Journal of Structural Geology, Vol 13, No 7, pp 837 to 850, 1991
Printed in Great Britain

0191-8141/91 $03 00+0 00

Experimental deformation of a quartz mylonite

S. RALSER*

Department of Earth Sciences, Monash University, Clayton, Victoria 3168, Australia

B. E. HOBBS and A. ORD

CSIRO, Division of Geomechanics, P.O. Box 54, Mt Waverly, Victoria 3154, Australia

(*Received* 20 *April* 1990; *accepted in revised form* 29 *January* 1991)

Abstract—Samples of a pure quartz mylonite have been axially shortened up to 60% in nickel capsules with water, at temperatures of 600–900°C, strain rates of 10^{-5}–10^{-7} s^{-1}, and a confining pressure of 1.64 GPa in a solid medium deformation apparatus. The mylonite was loaded in four orientations relative to the initial foliation and lineation: PSL, parallel to the foliation and lineation; 45SL, 45° to the foliation and lineation; NSL, normal to the foliation and lineation; and PSNL, parallel to the foliation, normal to the lineation.

The strength of the mylonite varies with the orientation of the specimen with respect to the loading direction, as well as with temperature and strain rate. Specimens deformed PSL are weakest, with those deformed 45SL slightly stronger, while specimens deformed NSL and PSNL are generally 200–400 MPa stronger. All experiments exhibit strain softening at strains greater than 15%.

Strongly flattened grains with sub-basal deformation lamellae are developed in all specimens, with the amount of recrystallization increasing as temperature is increased and/or strain rate is decreased.

The initial *c*-axis preferred orientation, typical of quartz mylonites, is an asymmetric girdle normal to the mylonitic foliation and lineation. In specimens deformed NSL and PSNL strengthening of the *c*-axis maximum parallel to the shortening direction is the major change in preferred orientation. The *c*-axes in these specimens are inferred to be in stable orientations with respect to the shortening direction. In specimens deformed PSL a new girdle develops parallel to the initial foliation, with subsidiary girdles running from the shortening direction to a position normal to the initial foliation and lineation. More complex fabrics observed in specimens deformed 45SL are associated with the triclinic symmetry of the overall deformation

The fabrics develop by initial kinking of grains, which have *c*-axes at high angles to the shortening direction, causing them to rotate into orientations more suitable for dislocation slip. Slip occurs on both basal and prism planes. Rhomb slip may have a minor influence. In all cases slip parallel to ⟨*a*⟩ is consistent with the observed fabrics. The complexity of the fabrics indicates that even at these high strains (60%) quartz can still show a memory for fabrics developed in previous deformations

INTRODUCTION

MOST metamorphic rocks are polydeformed. It is therefore important to examine the effect a pre-existing anisotropy has on deformation. The aim of this research was to investigate, over a range of orientations, temperatures and strain rates, the mechanical behaviour and the resultant microstructures and *c*-axis fabrics of experimentally deformed, strongly anisotropic material; in this case a quartz mylonite. This differs from the previous work of Green *et al.* (1970) and Tullis *et al.* (1973), both of whom used isotropic starting materials. The use of a mylonite allows the study of the mechanical effect of, and memory of, an initially strong anisotropy. The influence of a pre-existing anisotropy on the development of crystallographic preferred orientations has received surprisingly little attention in the geological literature. It has been suggested that an existing fabric can affect subsequently developed fabrics (Phillips 1945, Simpson 1980); this being especially true if there are no major changes in the operative slip systems (Evans & White 1984).

The effect of folding on mylonitic fabrics was addressed by Carreras *et al.* (1977). They show that for simple open folding, with no grain elongation parallel to the axial plane, fabrics are only passively rotated by the folding. Where significant grain growth occurs, a new fabric (similar to the old) develops symmetrically about the axial plane. In isoclinal folds the old fabric pattern is regenerated. The deformation of quartz 'blebs', showing an initially limited range in orientation of *c*-axes, results in non-reproducible fabrics (Van Roermund *et al.* 1979). The fabric developed depends on both the reorientation trajectories and the initial orientation distribution, with specific initial orientations feeding different maxima in the final fabric. Lister & Williams (1979) used the Taylor–Bishop–Hill model (see Lister *et al.* 1978) to study fabric development, where coaxial deformation follows earlier non-coaxial deformation, and the coaxial shortening is approximately normal to the *XY* plane (normal to the foliation). They conclude that (a) the asymmetry in the initial fabric is preserved as an asymmetric distribution in the resultant *c*-axis fabric, and (b) the fabric is sensitive to the change in kinematic framework, and the pattern migrates to reflect the new orientation, resulting in a pseudo-orthorhombic symmetry.

Experimental studies on the influence of an aniso-

* Present address: Centre for Deformation Studies in the Earth Sciences, Department of Geology, University of New Brunswick, Fredericton, N.B., Canada E3B 5A3.

tropy have been limited to marbles and agates (Griggs and co-workers, see Turner & Weiss 1963, Kern 1977, 1979, Rutter & Rusbridge 1977) rather than quartz mylonites Both Kern (1977, 1979) and Rutter & Rusbridge (1977) show that only comparatively low strains (less than 30% shortening) are necessary to obliterate any pre-existing fabric in marbles and agates.

The effect of initial anisotropy has received much more attention in materials science, and is particularly important in deformation processing for which it is necessary to produce specific fabrics (textures) for specific purposes. A strong initial fabric can have either a detrimental or a beneficial effect (Hosford & Backofen 1964, Avery *et al.* 1965, Backofen 1972, Sowerby & Johnson 1975). Two types of anisotropy are recognized: mechanical fibering (alignment of secondary phases) and crystallographic preferred orientation. The latter is considered the primary source of anisotropic behaviour Contrary to what has been observed in geological materials, evidence from metals suggests that the memory of an initial anisotropy (strong fabric) can be retained to very large strains (Mecking 1985).

STARTING MATERIAL

The specimen used in these experiments is a quartz mylonite with minor muscovite and trace tourmaline, collected from Little Broken Hill, near Broken Hill, New South Wales, where a pegmatite has been deformed in a shear zone. The mylonite shows a strong foliation and lineation, with the foliation defined by grain size changes. Mica plates are parallel to this foliation. Quartz grains are optically strain-free (Fig. 1); the grain size is variable, ranging up to 1 mm, but is commonly about 0.3 mm. Mica occurs throughout the specimen, both on quartz grain boundaries and within quartz grains. Universal stage measurements show that quartz *c*-axes have a strong preferred orientation (Fig. 2) with the development of an asymmetric girdle approximately normal to the foliation. Ideally the initial preferred orientation should be the same for each specimen; this was not possible in these experiments (Figs. 2b–d show some of the variation in *c*-axis preferred orientation in the initial mylonite).

Specimens were deformed in four orientations relative to the mylonitic foliation and lineation (Fig. 2); parallel to the foliation and lineation (PSL), normal to the foliation and lineation (NSL), parallel to the foliation, normal to the lineation (PSNL), and 45° to the foliation and lineation (45SL). Successful experiments were only completed for one of the two possible orientations in specimens deformed 45SL.

EXPERIMENTAL PROCEDURE

All experiments were conducted in a Tullis-modified Griggs solid medium deformation apparatus, using cold-pressed NaCl as the confining medium. The experimental procedure is nearly identical to that described by Ord & Hobbs (1986)

Temperature was controlled with a Eurotherm temperature controller connected to one thermocouple. Temperature, from a second thermocouple, load, pressure and displacement were recorded either on a continuous chart recorder, or via a data logger on to an HP85 microcomputer The load was corrected for elastic distortion of the rig, which was calculated by deforming a tungsten carbide specimen of known elastic properties. Stress was calculated on the current cross-sectional area, assuming homogeneous finite strain and no volume change Strain is based on the specimen dimensions at room pressure and temperature

Specimens were cored in a known orientation to the mylonitic foliation and lineation, and then ground on a diamond lap to a length of 12 or 15 mm. Specimens were placed in nickel jackets with 50 μl distilled water added. The capsules consist of a nickel cap hydrogen flame welded to each of two sections of nickel tube. These have a wall thickness of 0.2 mm and are constructed so one can slide, with a tight fit, inside the other, providing an 11 mm- or 14 mm-long metal–metal contact.

The capsule is surrounded by salt, as a confining medium, soft-fired pyrophyllite, a ramped graphite furnace, pyrophyllite and an outer salt piece (Fig. 3) Specimens were taken to experimental conditions within 3 h. The specific volume for water was kept below that required to rupture the capsule during both the loading and unloading histories of the experiments. All specimens deformed at strain rates of 10^{-5} and 10^{-6} s^{-1} were

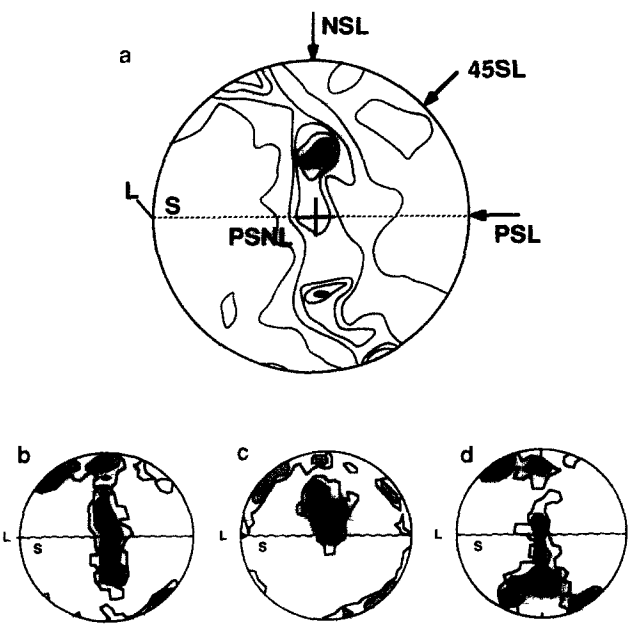

Fig 2 Initial *c*-axis preferred orientation: (a) measured manually on a universal stage (200 points, 5, 4, 3, 2 and 0.5%/1% area, equal area), showing orientations used in these experiments. NSL—deformed normal to the foliation and lineation; 45SL—deformed at 45° to the foliation and lineation, PSL—deformed parallel to the foliation and lineation; PSNL—deformed parallel to the foliation, normal to the lineation (b)–(d) Variation in *c*-axis preferred orientation which can occur between different specimens (measured using photometric method, based on 150 grain orientations, 4, 2 and 0.67%/0.67% area)

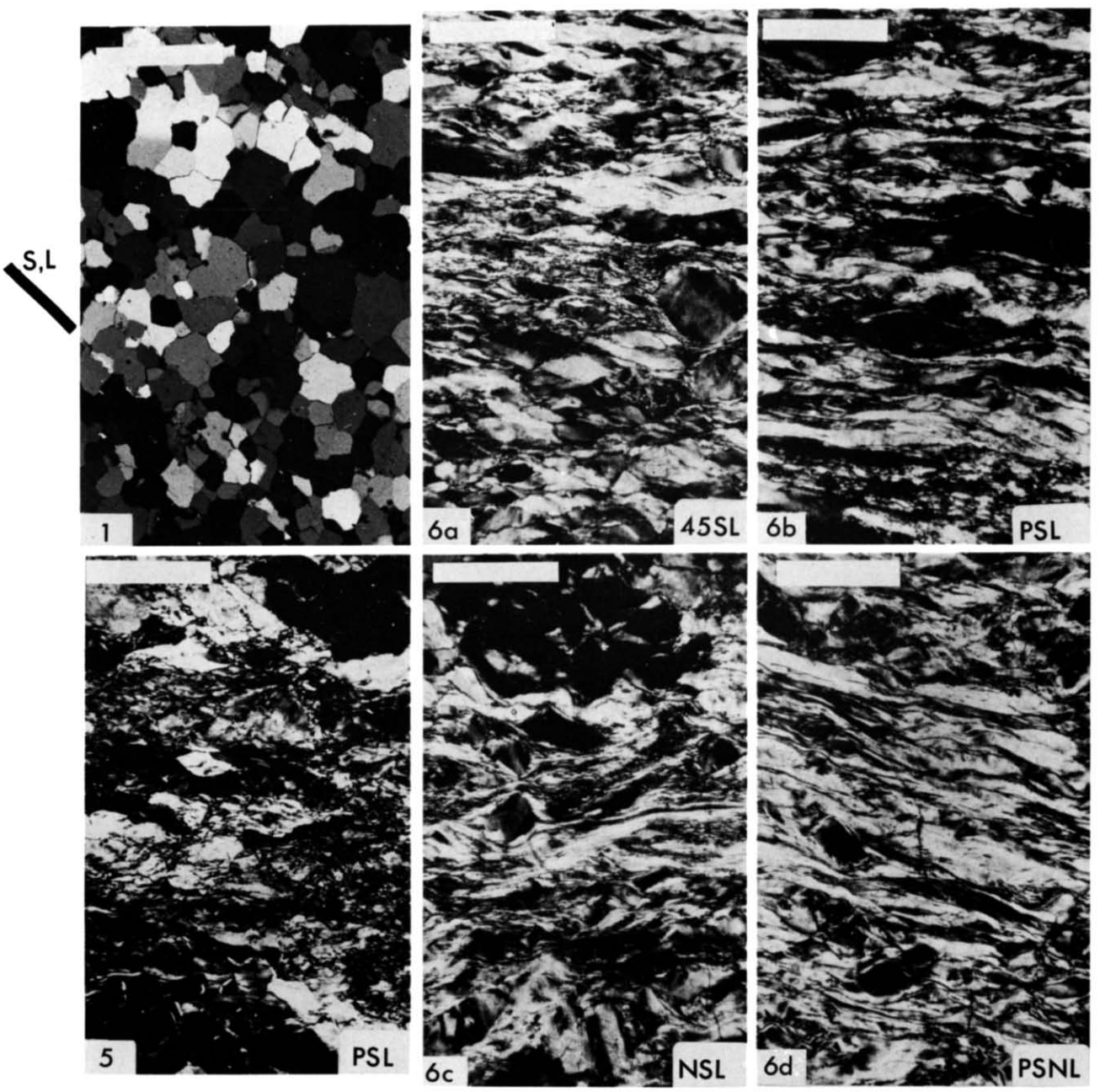

Fig 1 Initial microstructure of the quartz mylonite. The mylonitic foliation (S) is normal to the plane of the figure and the mylonitic lineation (L) is in the plane of the figure. (Scale bar: 1 mm).

Fig. 5. Microstructure developed in G0318 (PSL, 700°C, 10^{-5} s^{-1}), a specimen showing no recrystallization. Kink bands are prominent in many grains (scale bar: 200 μm). (Note—In all photomicrographs the shortening direction is N–S Except where indicated, the mylonitic foliation is normal to the photo; in specimens deformed 45SL, PSL and NSL the mylonitic lineation is in the plane of the page, in specimens deformed PSNL the lineation is normal to the page.)

Fig 6 Microstructures developed in specimens for the different orientations deformed at 700°C, 10^{-6} s^{-1}: (a) G0193, 45SL; (b) G0248, PSL; (c) G0342, NSL; (d) G0254, PSNL (scale bar: 200 μm).

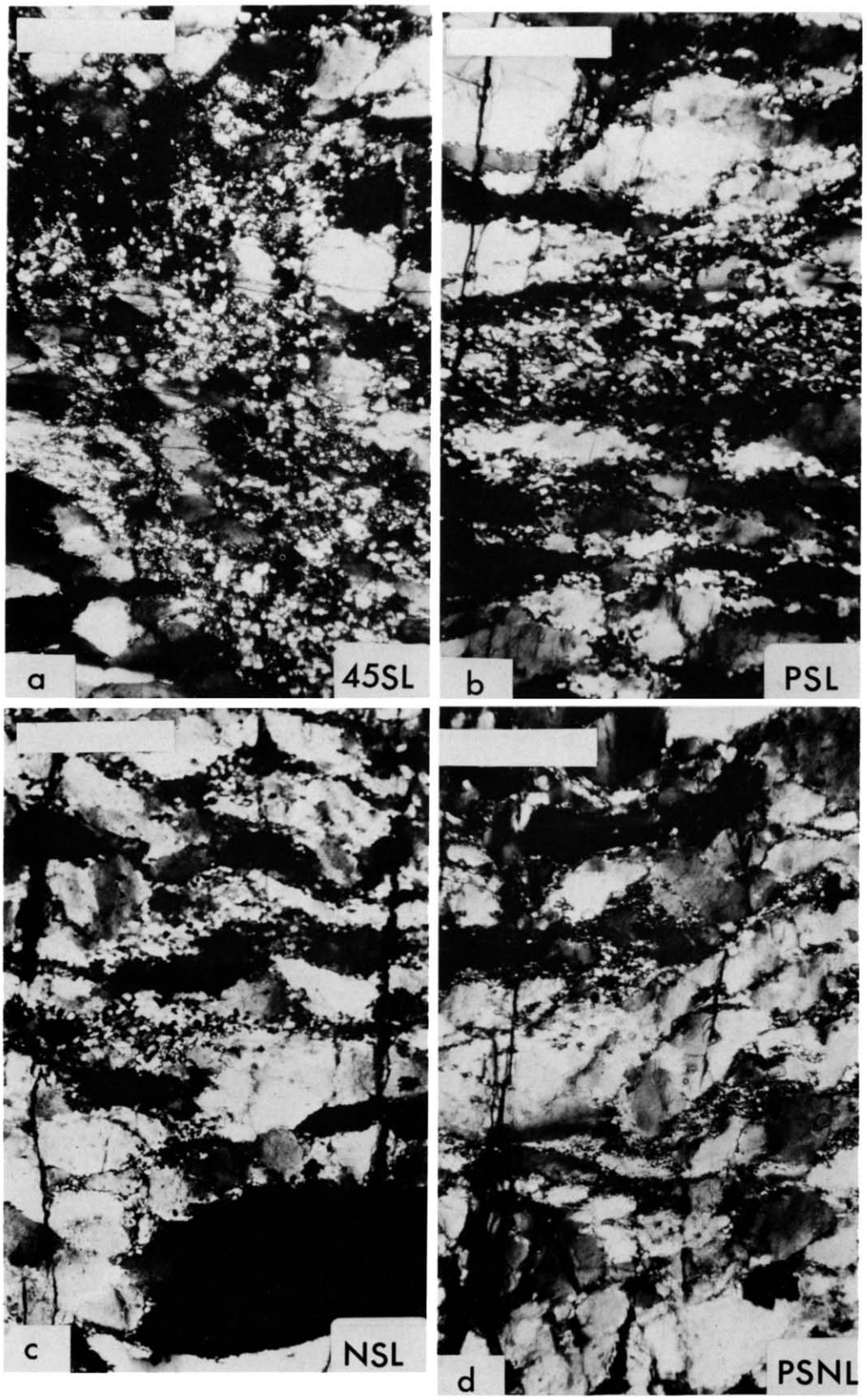

Fig. 7. Microstructures developed in specimens for the different orientations deformed at 900°C, 10^{-6} s^{-1}. (a) G0226, 45SL; (b) G0338, PSL; (c) G0340, NSL; (d) G0339, PSNL (scale bar: 200 μm)

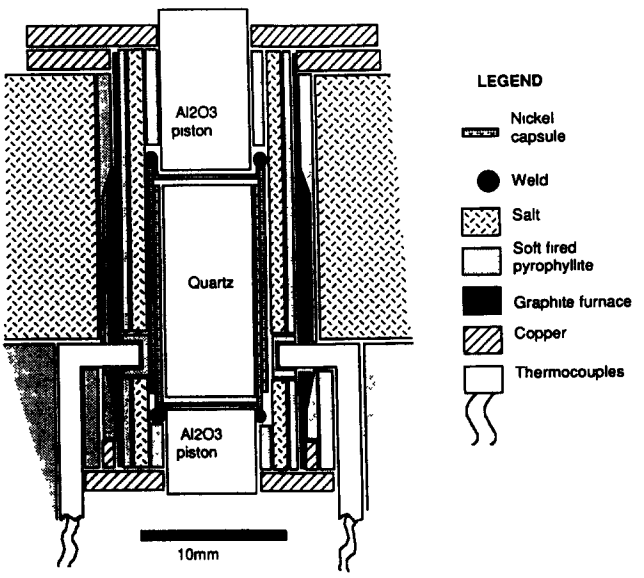

Fig. 3. Sample assembly (after Ord & Hobbs 1986).

kept at pressure and temperature for between 20 and 30 h prior to deformation commencing.

At the completion of an experiment specimens were impregnated with a low viscosity epoxy resin through areas where the nickel had been removed. The remaining nickel was dissolved off in 70 weight percent HNO_3. The specimens were then mounted in epoxy and cut in half. Deformed specimens were cut in the plane containing the thermocouples; parallel to the initial foliation for specimens deformed PSL and PSNL, and parallel to the initial lineation for specimens deformed NSL. The specimens deformed 45SL were cut normal to the initial foliation.

The two differences between the experimental procedure used here and that used by Ord & Hobbs (1986) are: (a) Ni capsules with water added are used, rather than Ag capsules with water and buffer; and (b) specimens were kept for up to 30 h at pressure and temperature prior to deformation (compared with 20 h).

Experimental conditions

Experiments were conducted at a nominal confining pressure of 1640 MPa, temperatures of 600–900°C, and initial strain rates of 1.35×10^{-5}, 1.35×10^{-6} and 1.35×10^{-7} s^{-1} (Table 1). Differential stresses ranged up to 1900 MPa, with sample shortening of up to 65%. Maximum longitudinal strains ranged up to 95% in the central, deformed portions of some specimens. The strength of the nickel jacket has not been taken into account. Kronenburg & Tullis (1984) use stress corrections of 10 MPa at temperatures greater than 900°C, and up to 100 MPa at 700°C, for nickel sleeves with a wall thickness of 0.6 mm. Smaller stress corrections would be necessary in these experiments as the wall thickness is less (0.4 mm). The relative strengths of the four specimen orientations used here (at the same temperature) are not dependent on correcting the stress for the jacket strength.

The oxygen fugacity in the Ni jackets with water added is 10^{-15} MPa (at 800°C, 1.64 GPA), one order of

Table 1. Experimental conditions for specimens described in this paper. Notes: PSL—deformed parallel to the foliation and lineation, NSL—deformed normal to the foliation and lineation, PSNL—deformed parallel to the foliation, normal to the lineation, 45SL—deformed 45° to the foliation and lineation; % strain—measured shortening of specimen; maximum longitudinal strain—measured maximum longitudinal strain (for specimens deformed PSL this is normal to the original lineation in the plane of the original foliation, for NSL and PSNL this is parallel to the original lineation); G0194 failed by sliding on the foliation

Strain rate ($\log s^{-1}$)	Temp. (°C)	Orientation	Confining pressure (MPa)	% strain	Maximum longitudinal strain	Stress 10% strain (MPa)	Run No.
−5	700	45SL	1625	36	—	1540	G0194
	700	PSL	1600	37	41	1170	G0318
	800	45SL	1620	40	45	680	G0195
	800	PSL	1650	57	93	1200	G0251
	800	NSL	1650	46	49	910	G0223
	800	PSNL	1500	51	47	950	G0225
	800	45SL	1650	53	70	320	G0212
	900	PSL	1650	47	65	450	G0214
	900	NSL	1650	34	44	890	G0217
	900	PSNL	1675	54	56	385	G0224
−6	600	PSL	1600	46	49	1100	G0343
	700	45SL	1680	54	58	480	G0193
	700	NSL	1600	49	64	880	G0342
	700	PSL	1655	73	85	450	G0248
	700	PSNL	1640	66	85	790	G0254
	800	45SL	1615	58	52	400	G0241
	800	PSL	1670	56	66	270	G0233
	800	NSL	1670	64	82	580	G0257
	800	PSNL	1670	65	78	600	G0259
	900	45SL	1680	46	39	225	G0226
	900	PSL	1600	49	59	180	G0338
	900	PSNL	1600	33	44	220	G0339
	900	NSL	1600	37	48	220	G0340
−7	700	PSL	1490	33	33	200	G0231

magnitude lower than that buffered by Ni–NiO (Davidson personal communication 1986). Such chemical conditions are similar to those obtained using the QFM buffer, commonly used by experimental petrologists to model crustal conditions.

SPECIMEN STRENGTH

In these experiments, specimen strength varies with changing temperature, strain rate and orientation. The effects of varying temperature and strain rate has received considerable attention, with quartzites initially studied in detail by Green *et al.* (1970) and Tullis *et al.* (1973). These and other studies show that strength decreases with increasing temperature and/or decreasing strain rate. Similar trends are observed here (Fig. 4).

Specimens deformed PSL are generally the weakest (Fig. 4). However no real distinction is possible between specimens in this orientation and those deformed 45SL. Specimens in this group (both PSL and 45SL) are generally 200–400 MPa weaker than specimens deformed NSL and PSNL, and are best illustrated by the sets of experiments at 700°C (Fig. 4) and 800°C (Fig. 4), at a strain rate of 10^{-6} s^{-1}

Group distinctions are not possible at 900°C (Fig. 4), where the strength of all specimens is approximately similar (especially for those specimens deformed at 10^{-6} s^{-1}) It is not known whether such isotropic behaviour is only a function of lack of discrimination of the load cell or whether it is real and will continue at higher temperatures and/or lower strain rates.

Exceptions to the above trends exist; the most notable of which is the specimen deformed PSL at 800°C and 10^{-5} s^{-1} (Fig. 4, Run G0251). This specimen shows an anomalously high strength, with a large stress drop between 15 and 30% strain. Thin-section examination of this specimen shows that strain was not accommodated homogeneously, and is concentrated at one end of the specimen. Microstructures and *c*-axis preferred orientations for this specimen are described in detail in Ralser (1990), and will not be discussed further in this paper (and should be ignored in comparing the relative strengths).

Very few experiments attain steady state; most specimens show appreciable amounts of strain softening. This strain softening occurs in two ways; a sudden stress drop between strains of 15 and 30% (e.g. most specimens at 800°C and 10^{-5} s^{-1}) and/or a steady stress drop with increasing strain (e.g. most specimens). This strain

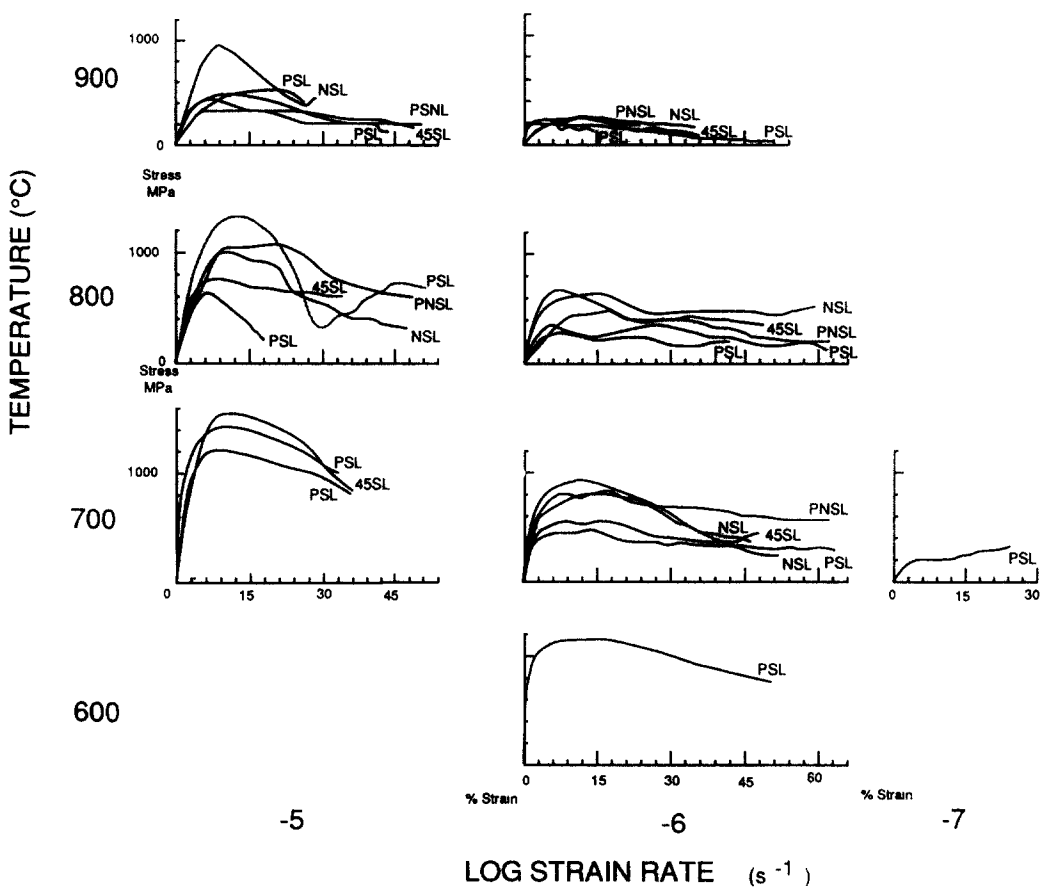

Fig. 4. Stress–strain curves for all specimens for varying temperature and strain rate (PSL—shortened parallel to the foliation and lineation; NSL—shortened normal to the foliation and lineation; 45SL—shortened 45° to the foliation and lineation; PSNL—shortened parallel to the foliation and normal to the lineation.) Not all specimens are listed in Table 1 One specimen deformed PSL (shaded in grey) in the set at 800°C and 10^{-5} s^{-1} is anomalously strong. This specimen should be ignored when comparing relative strengths

softening may result from strain being accommodated on shear zones, which are present in a number of specimens (see Ralser 1990 for more detail).

SPECIMEN SHAPE

Specimens deformed NSL and PSNL show greater strain parallel to the lineation than normal to the lineation, while specimens deformed PSL show greater strain normal to the lineation, in the plane of the initial foliation. Specimens deformed 45SL display more homogeneous barrelling.

MICROSTRUCTURES

The microstructures developed vary with both temperature and strain rate. Flattened grains, with abundant sub-basal deformation lamellae, dominate. The number of recrystallized grains increases with increasing temperature and/or decreasing strain rate, with the orientation of the specimen having little effect on the developed microstructures. The microstructures developed are similar to those produced in the experiments of Green *et al.* (1970) and Tullis *et al.* (1973).

Many specimens develop shear zones at 30–40° to the shortening direction, most of which are recrystallized (Ralser 1990). At low strains (up to 30%) most of the deformation is accommodated within these shear zones, with only minor flattening of grains in the bulk of the specimen. At higher strains, the deformation cannot be fully accommodated by movement along the shear zones, so deformation occurs throughout the rest of the specimen. It is the microstructures developed at this stage that are described in this paper. As strain is further increased the piston punches into the specimen, and material is sheared past the corner of the piston (see Ralser 1990).

The only specimens deformed at the fastest strain rate and/or lowest temperature used in this study are shortened PSL (G0343—600°C, 10^{-6} s^{-1}; G0318—700°C, 10^{-5} s^{-1}, Fig. 5). Specimens deformed 45SL at these conditions fail by sliding on the foliation (e.g. G0194), whereas the ultimate strengths of the specimens in the other orientations (NSL, PSNL) would exceed the strength of the tungsten carbide load piston. The specimens deformed PSL (G0318, G0343) show no recrystallization. The deformed zones in the specimens are characterized by strongly flattened grains. Deformation bands are strongly developed within most grains, and are symmetrically oriented about the shortening direction (Fig. 5).

Deformation in the remainder of the specimens is accommodated by flattening of grains accompanied by grain boundary recrystallization. Figures 6 and 7 illustrate developed microstructures for two sets of conditions (Fig. 6—700°C, 10^{-6} s^{-1}; Fig. 7—900°C, 10^{-6} s^{-1}). As temperature is increased and/or strain rate is decreased the amount of recrystallization increases, with recrystallized grains becoming more equant and larger (Fig. 7) in specimens showing lower flow stresses. This recrystallized grainsize varies with the strength of the specimen, and hence orientation. Specimens deformed PSL and 45SL show larger recrystallized grains than the specimens deformed NSL and PSNL (compare grainsize in Figs. 7a & b with that in Figs. 7c & d).

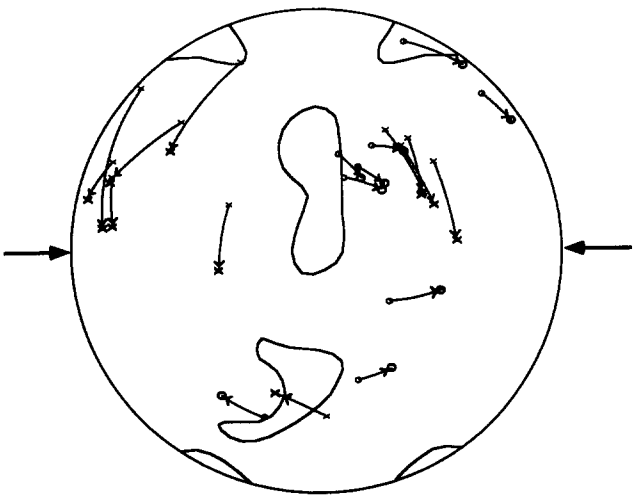

Fig. 8 *c*-axis orientations either side of deformation band boundaries in specimens deformed PSL. Crosses are from G0248, circles are from the less deformed G0297; bold character indicates orientation of kinked portion of grain. (N.B. These measurements are biased towards grains with *c*-axes in the cross-girdle.) Solid lines delimit areas with concentrations greater than 3%/1% area in the initial fabric.

All specimens show the development of kink bands in many grains. These kink bands have their boundaries parallel to the *c*-axis and are best observed in grains with *c*-axes on the perimeter of the stereonet. Grains with *c*-axes furthest from the shortening direction show the best development of kink bands. Kinking, in all cases, causes the *c*-axes in the deformed portions of the grains to move closer to the shortening direction (Fig. 8).

c-AXIS PREFERRED ORIENTATIONS

c-axis preferred orientations have been measured in all specimens using the photometric method of Price (1979). This has the advantage of measuring the *c*-axis preferred orientation simultaneously for all grains in the complete field of view, which is not possible with conventional universal stage techniques.

The initial *c*-axis fabric in these specimens is an asymmetric girdle normal to the mylonitic foliation (Fig. 2), typical of those found in greenschist facies mylonite zones throughout the world. Such fabrics generally consist of a skeleton (the girdle) containing three *c*-axis maxima. The skeleton of the initial *c*-axis girdle is essentially constant, although the location and intensity of the maxima may vary between individual specimens (Fig. 2). An indication of the orientation of the initial girdle, and location and intensity of the maxima can be obtained from the undeformed end regions of the speci-

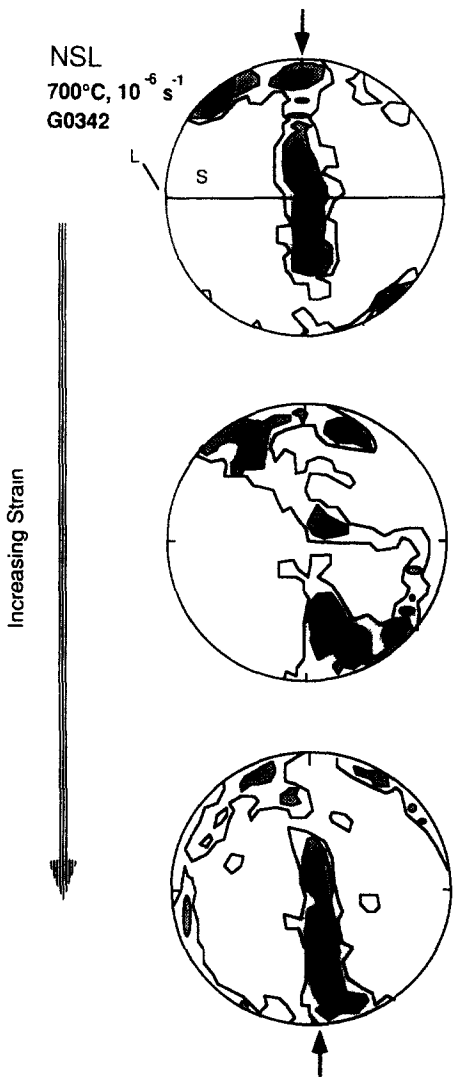

Fig. 9 *c*-axis fabrics developed in G0342 (NSL, 700°C, 10^{-6} s^{-1}, 49% strain). A general note for all figures showing fabrics. *c*-axis fabrics are shown for increasing strain, from less deformed to more deformed areas in the same specimen. All fabrics are measured using the photometric technique, and are calculated on 150 orientations; contours—4, 2 and 0.67%/0 67% area, equal-area projections. The initial orientations of the foliation and lineation are superimposed on the fabrics from the less deformed areas

mens. Figures 9–12 show *c*-axis fabrics with increasing strain, from less deformed to more deformed regions within the same specimen. The presence or absence of a given maximum between diagrams in the same specimen reflects the variation in *c*-axis fabric within the initial mylonite.

Specimens deformed NSL

Specimens deformed NSL have the deformation axes symmetrically imposed with respect to the specimen's foliation and lineation, with the initial orientation of *c*-axes at a low angle to the shortening direction. The specimens deformed in this orientation show little change in *c*-axis preferred orientation with increasing strain. Girdles become depopulated (Fig. 9), while the maxima become more intensified. A secondary, though minor, trend is to distribute *c*-axes more evenly about the shortening direction. The presence or absence of individual maxima with increasing strain reflects the *c*-axis distribution in the undeformed specimen. No significant variations are observed with changing temperature or strain rate.

This is consistent with the theoretical study of Lister & Williams (1979). These experimental results differ slightly in that there is no major trend towards the orthorhombic symmetry observed in the theoretical study. Importantly, as observed by them, the asymmetry of the starting material is still observed after high coaxial strains (e.g. up to 65% shortening in G0257).

Specimens deformed PSNL

Fabrics developed in specimens deformed PSNL are similar to those deformed NSL; namely, there is no significant change in *c*-axis preferred orientation with deformation. This is illustrated in Fig. 10 (G0254, 700°C, 10^{-6} s^{-1})

Specimens deformed PSL

Specimens deformed PSL show a major change in *c*-axis preferred orientation. Although the deformation axes are symmetrically imposed with respect to the specimen's foliation and lineation, the initial orientation of *c*-axes is at a high angle to the shortening direction.

In general the *c*-axis fabric which develops is best described as an asymmetric girdle parallel to the short-

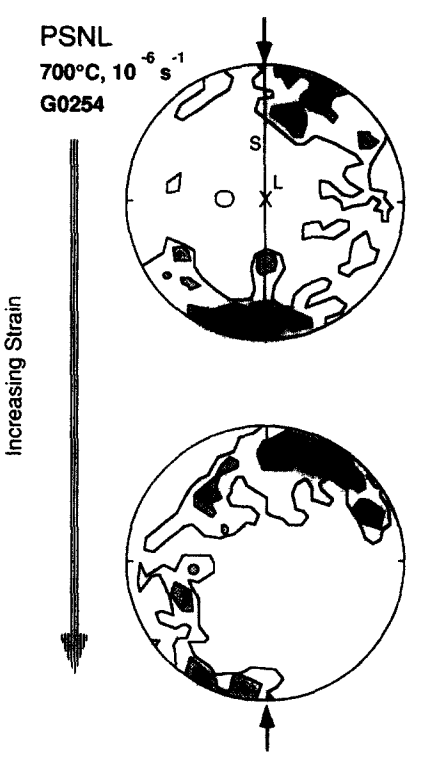

Fig. 10 *c*-axis fabrics developed in G0254 (PSNL, 700°C, 10^{-6} s^{-1}, 66% strain). See Fig 9 for comments

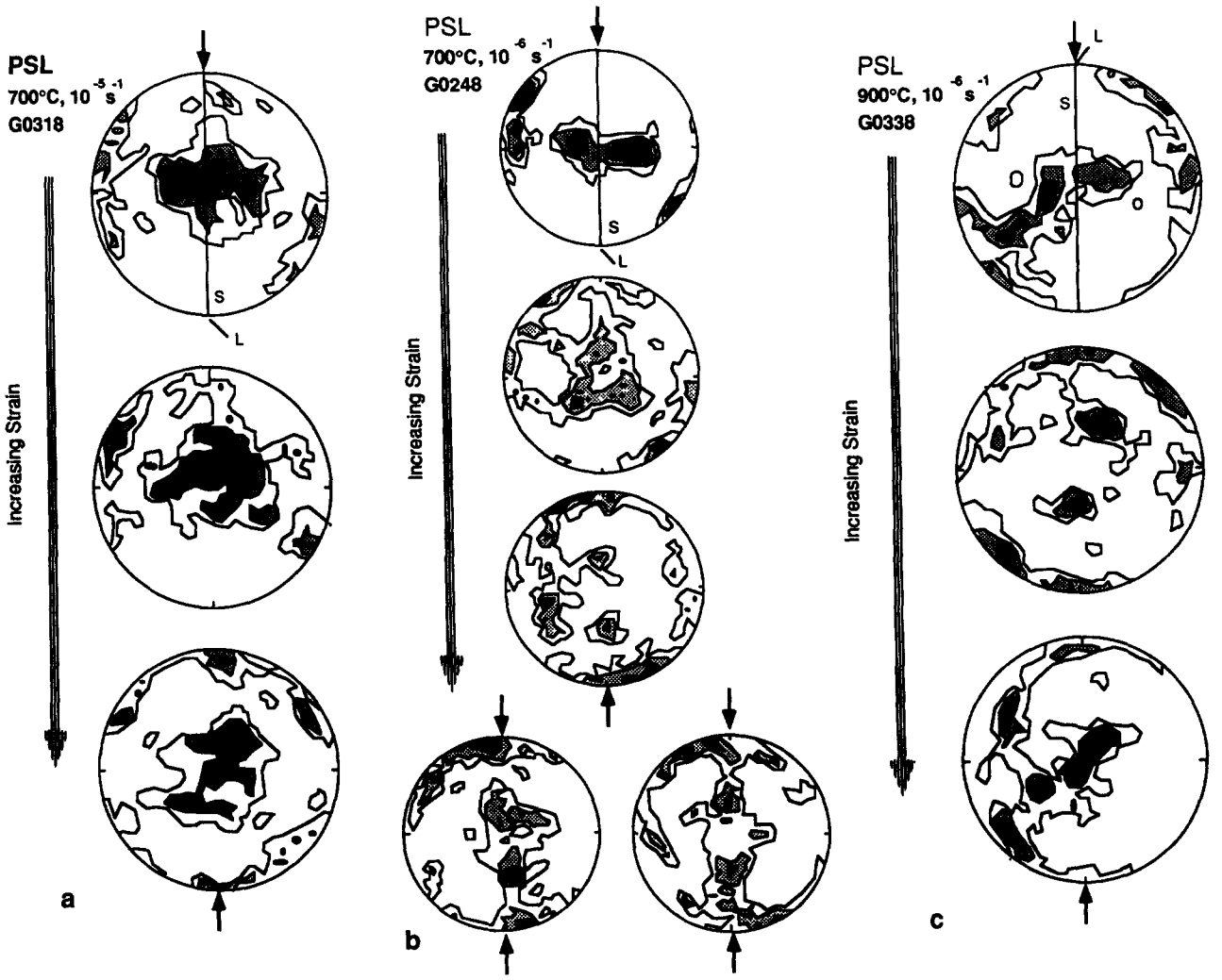

Fig. 11. c-axis fabrics developed in specimens deformed PSL. (a) G0318 (PSL, 700°C, 10^{-5} s^{-1}, 37% strain); (b) G0248 (PSL, 700°C, 10^{-6} s^{-1}, 73% strain); (c) G0338 (PSL, 900°C, 10^{-6} s^{-1}, 49% strain). See Fig 9 for comments.

ening direction (Fig. 11, best seen in Fig. 11b). It consists of a maximum (on the perimeter) at or near the shortening direction, with partial girdles extending towards the normal to the initial foliation. Two maxima develop between the shortening direction and the normal to the initial lineation in the plane of the initial foliation. These maxima are connected by a girdle parallel to the shortening direction. This development is best illustrated in G0248 (700°C, 10^{-6} s^{-1}, Fig. 11b). The two maxima in the plane of the initial foliation are not always equidistant from the shortening direction; in G0248 one maximum is approximately 40°, and the other approximately 50° from the shortening direction.

The positions of the maxima vary with changing temperature and strain rate (compare G0318, Fig. 11a, deformed at a lower temperature than G0248, Fig. 11b, and G0338, Fig. 11c). This is illustrated by the positions of maxima closest to the shortening direction. In G0318 a *c*-axis maximum is developed nearly parallel to the shortening direction; in G0248 the maximum is approximately 10° from the shortening direction; and in G0338 the maximum is approximately 40° from the shortening direction.

The specimens deformed at the 'coldest' conditions (e.g. G0318, 700°C, 10^{-5} s^{-1}, Fig. 11a) show no recrystallization (Fig. 5). This specimen is also deformed to lower strains than the specimens deformed at higher temperatures (Table 1). A strong maximum is developed near the shortening direction. This maximum is not on the perimeter, and may result from not having a maximum on the perimeter of the starting material. The maximum, in the centre, is initially elongate normal to the original foliation. With increasing strain this maxima contracts normal to the initial foliation, and spreads towards the shortening direction. In the most deformed portion of the specimen this 'girdle' starts to split into two maxima. These two maxima remain at a high angle to the shortening direction.

Specimens G0248 and G0338 are deformed to high strains (Table 1) and show well developed fabrics. In specimen G0248 (700°C, 10^{-6} s^{-1}; Fig. 11b) fabric changes can be mapped from low to high strain areas. Although an initial fabric could not be measured, it is inferred to be a girdle showing a dextral sense of asymmetry. At low strains there is movement of the maximum on the perimeter towards the shortening direction. Simultaneously with the movement of this maximum, there is a reduction in the width (normal to the initial

foliation) of the maxima in the centre, with movement of *c*-axes towards the shortening direction. This movement of *c*-axes leads to a fabric pattern in the most deformed zones, which is best described as an asymmetric girdle parallel to the shortening direction. Similar fabric trends are observed in the specimen showing significant recrystallization (G0338, 900°C, 10^{-6} s^{-1}; Fig. 11c). *c*-axis maxima (in G0338), apart from a maximum close to the shortening direction, are further from the shortening direction than for the previous specimens

Specimens deformed 45SL

In specimens deformed 45SL the deformation axes are not symmetrically imposed on the specimen's axes of anisotropy. The resulting fabric may be expected to be—and is—less symmetrical than in the other orientations deformed in this study

Although specimens deformed 45SL show changes in fabric, no consistent differences are observed over the range of experimental conditions (700–900°C, 10^{-5}–10^{-6} s^{-1}).

Three major fabric changes which occur in one of these specimens (Fig. 12; G0193, 700°C, 10^{-6} s^{-1}) are:

(1) the maximum on the perimeter rotates towards the shortening direction;
(2) *c*-axes in the centre move towards the shortening direction;
(3) a minor maximum develops at a high angle to the shortening direction.

In summary, two of the orientations (NSL, PSNL) show little change in the initial fabric with deformation. The fabrics developed exhibit little variation with changes in temperature and strain rate. Specimens deformed in these orientations (NSL, PSNL) are the stronger of the four orientations used in this study. The specimens deformed PSL show large changes in fabric consistent with variation in temperature and strain rate, with a *c*-axis girdle developed parallel to the shortening direction. The final orientation deformed in this study (45SL) shows large changes in fabric, but no systematic variation with temperature and strain rate.

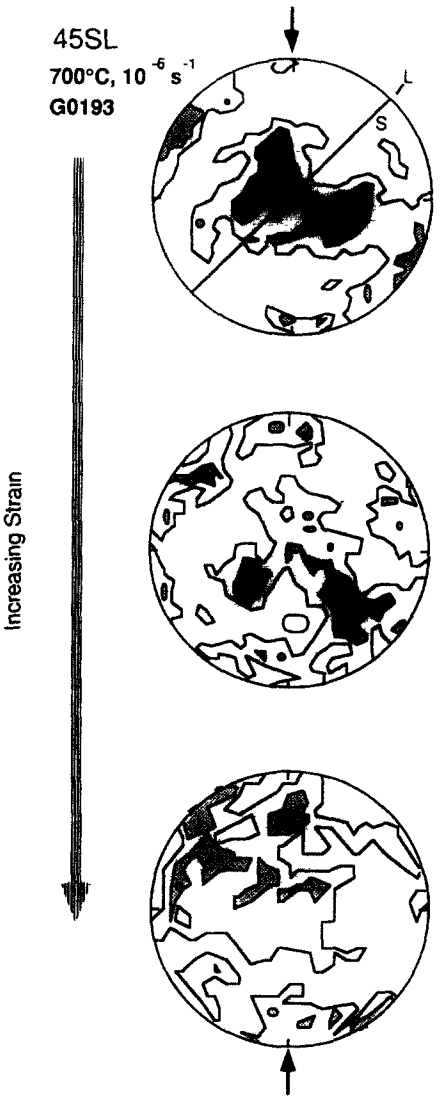

Fig 12 *c*-axis fabrics developed in G0193 (45SL, 700°C, 10^{-6} s^{-1}, 54% strain). See Fig 9 for comments

DISCUSSION

Origin of the preferred orientation

All specimens described here show the development of a strong crystallographic preferred orientation during experimental deformation. This indicates that dislocation slip was the major strain-accommodating mechanism. This is further supported by the presence of highly flattened grains showing well developed deformation lamellae. It is therefore necessary to make some estimate of the operative slip system. Numerous slip systems have been identified in quartz, principally through transmission electron microscopy, recognition of deformation lamellae, and the identification of the orientation of slip bands on polished surfaces of specifically oriented, deformed single crystals (see table 1, Linker *et al.* 1984).

Schmid & Casey (1986) determined the complete preferred orientations of quartz grains in a number of natural quartzites showing a variety of *c*-axis fabrics. They were able to identify the operating slip systems by observing which crystallographic directions were parallel to the inferred flow direction, and which crystallographic planes were parallel to the inferred flow plane. They have shown that their observations are consistent with the $\langle a \rangle$ direction being the only operative slip direction, with slip occurring on the basal, prism, and positive and negative rhomb planes. This will be accepted here. The use of only these slip systems is insufficient to allow homogeneous deformation using the strict Von Mises criterion, which requires the operation of five independent slip systems, including operation of the hard $\langle c \pm a \rangle$ slip system. Recently it has been shown that this can be relaxed for special conditions, allowing homogeneous deformation on fewer slip systems (Kocks & Canova 1981, Kocks & Chandra 1982). The development of flat grains constrains the strains

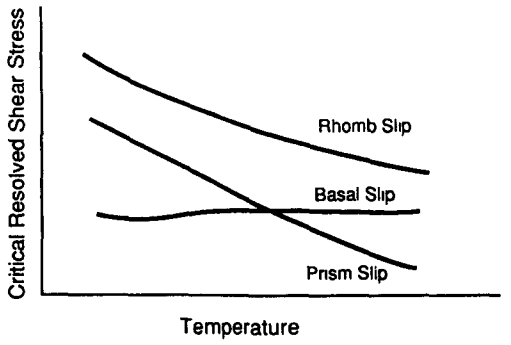

Fig. 13 Schematic plot of critical resolved shear stress vs temperature for basal, prism and rhomb slip (after Hobbs 1985).

imposed across the flat grain boundaries to be the same. The strains can still vary across the much smaller end boundaries. This allows homogeneous deformation, at least within the centre of each grain, on fewer slip systems.

Tullis *et al.* (1973) showed that the increase in angle between the shortening direction and the *c*-axis small circle girdle can be attributed to increased prism slip. It has also been shown in single crystal experiments that prism slip becomes easier than basal slip at higher temperatures (Blacic 1975, Linker *et al.* 1984).

In order for slip to occur, the shear stress resolved on the slip system must reach a critical value (the critical resolved shear stress, CRSS). Variations in this stress are controlled by a number of factors, the principal of which are temperature and strain rate (Blacic 1975, Linker *et al.* 1984 review this for quartz). Increasing temperature and/or decreasing strain rate will decrease the CRSS, but the amount of change in CRSS is different for different slip systems (Fig. 13) (Hobbs 1985). At high temperatures prism slip has a lower CRSS than basal slip. Blacic (1975) shows this transition from dominantly basal slip to dominantly prism slip occurs at temperatures of 700–800°C, at experimental conditions like those used in the experiments described in this paper (although we must accept the results of single crystal experiments and extrapolate them to polycrystals). The relative CRSS for rhomb ⟨*a*⟩ slip is not known, although it will be lower than that for ⟨*c* ± *a*⟩ slip (Linker *et al.* 1984). In the following discussion it is assumed to be stronger than both basal and prism slip.

If, as inferred from the work of Blacic (1975), the CRSSs for basal and prism slip are approximately equal (at the experimental conditions used in the experiments described in this paper), the fabrics developed in the specimens described in this paper will depend only on the magnitude of the resolved shear stresses acting on the different slip systems (i.e. Schmid factor). Slip will occur first on those systems having the highest Schmid factor (e.g. Hobbs 1985, Van Houtte & Wagner 1985). As the CRSS will not depend on the orientation of the specimen, at any one set of experimental conditions, the fabrics that develop will depend only on the Schmid factors for the slip systems present.

Schmid factors (Table 2) are calculated for five ideal-

Table 2 Schmid factors for five ideal crystal orientations, indicated in Fig. 14 These are calculated assuming ⟨*a*⟩ slip, with an *a*-axis on the perimeter, normal to the *c*-axis girdle (parallel to the mylonitic lineation). Numbered positions refer to Fig. 14 (1, 2, 3—maximum A; 4, 5—maximum B. Maxima A and B are referred to in the text)

		Specimen orientation			
Position	Slip plane	PSL	45SL	NSL	PSNL
1	Basal	0 00	0.41	0.44	0 45
	Prism	0.43	0.32	0.15	0.16
	Rhomb	0.35	0.50	0 39	0.50
2	Basal	0 00	0.30	0.42	0.41
	Prism	0.42	0.45	0.31	0.17
	Rhomb	0.35	0.43	0.50	0.38
3	Basal	0 00	0.16	0.27	0.21
	Prism	0.40	0.50	0.42	0.03
	Rhomb	0.39	0.49	0.49	0.21
4	Basal	0.28	0.44	0.26	0.00
	Prism	0.42	0.34	0.03	0.43
	Rhomb	0.42	0.39	0.17	0.18
5	Basal	0 45	0.24	0.46	0.00
	Prism	0.31	0.41	0.12	0.43
	Rhomb	0.38	0.39	0.28	0.18

ized single crystal orientations (Fig. 14) to represent the initial *c*-axis fabric of the starting material. This calculation assumes a strong ⟨*a*⟩ maximum normal to the girdle, parallel to the mylonitic lineation, consistent with the data of Schmid & Casey (1986). The Schmid factors for positive and negative rhombs have not been separated. Although Schmid factors for rhomb slip are high, the CRSS for rhomb slip is also high. Slip on basal and/or prism planes is therefore considered to be of greater importance than slip on rhomb planes.

Specimens deformed NSL

Specimens deformed NSL show little change in preferred orientation as *c*-axes are already in a stable orientation with respect to the shortening direction. The theoretical study of Lister & Hobbs (1980, fig. 16H) shows that grains which initially have their *c*-axes in stable orientations show low reorientation rates com-

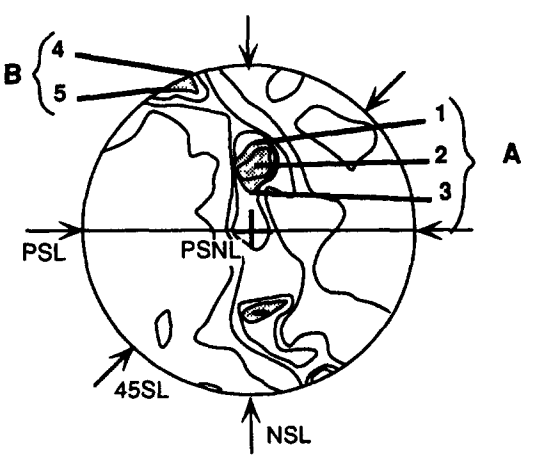

Fig. 14. Initial *c*-axis preferred orientation, showing orientations of ideal crystal locations used for calculating the Schmid factors in Table 2. A and B are maxima referred to in the text

pared to grains in unstable orientations. A similar result was obtained theoretically using the Taylor–Bishop–Hill model (Lister & Williams 1979). In the experiments described in this paper the maxima become intensified as strain is increased, with a strong maximum developing near the shortening direction. This reflects both the high Schmid factor for basal slip and the orientation of the deformation bands in grains from maximum B (Fig. 14 and Table 2). The deformation of grains in maximum A (Fig. 14) reflects a stable interaction of basal, prism and rhomb slip. Rhomb slip (having a high Schmid factor) may be relatively important, as rhomb planes in grains in this orientation show a significantly higher Schmid factor than grains in maximum B. This is consistent with the data of Schmid & Casey (1986), who show that for grains having orientations in maximum A, the rhomb planes also have a strong preferred orientation.

Specimens deformed PSNL

Specimens deformed PSNL are similar to those deformed NSL in showing little change in preferred orientation with deformation. Grains in maximum B have a Schmid factor of zero on the basal planes, and high Schmid factors on the prism plane. Such grains deform predominantly on the prism plane, leading to a strong maximum normal to the shortening direction. Deformation of maximum A is controlled by balanced basal and rhomb slip, as both systems have high Schmid factors. Many grains are unsuitably oriented for slip. These deform initially by the formation of deformation and kink bands. With increasing strain, deformation is accommodated by recrystallization in these bands.

Specimens deformed PSL

It is not possible to explain the fabrics developed in specimens deformed PSL simply by dislocation slip, and the widespread development of deformation bands has to be considered. Most grains from maximum B which are closer to the shortening direction are suitably oriented for basal ⟨*a*⟩ slip (positions 4, 5 in Table 2), as they have high Schmid factors for this slip system. However, at lower strains kink bands, subparallel to *c*-axes, are well developed in many grains. These kink bands, best developed in grains further from the shortening direction than those from the vicinity of positions 4 and 5 (which have a high Schmid factor for prism slip), effectively rotate *c*-axes in portions of the grains closer to the shortening direction (Fig. 8). This permits deformation to continue easily by basal slip, especially in grains where prism ⟨*a*⟩ slip would otherwise be expected to play an important role (indicated by Schmid factors from Table 2).

The situation is not nearly as simple for grains in maximum A. None of the slip systems (or combinations) will lead to the observed *c*-axis fabrics (e.g. G0248, Fig. 11b). There is a Schmid factor of zero for basal slip; *c*-axes will remain essentially stationary for prism slip, and will rotate approximately towards the shortening direction for rhomb slip. If deformation occurs primarily by rhomb ⟨*a*⟩ slip during the early stages of deformation, *c*-axes will rotate towards the shortening direction (Fig. 15b). In this new orientation prism slip, with a high Schmid factor, will rotate *c*-axes back to approximately their original position, while basal slip (if operative) will rotate *c*-axes towards the shortening direction (Fig. 15d). In such a situation the *c*-axis girdle which develops would be in the plane containing the shortening direction and maximum A. This is not observed.

Kink bands are also observed in grains from maximum A. The operation of these kink bands results in larger jumps in *c*-axis orientation (Figs. 8 and 15c) than from purely dislocation slip. This larger movement towards the shortening direction (Fig. 15c) changes the prism plane having the highest Schmid factor (Fig. 15e). Slip

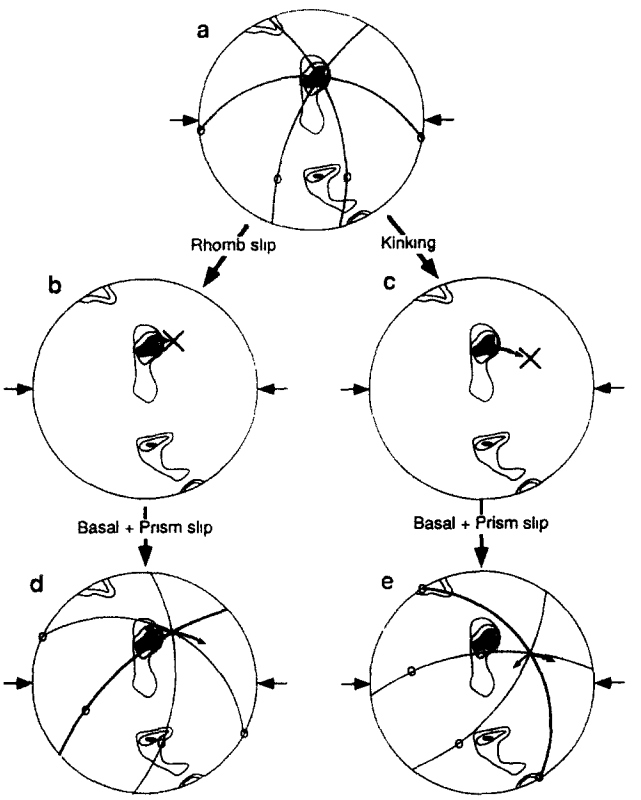

Fig 15 *c*-axis reorientation paths; great circles indicate orientation of prism planes, circles indicate orientation of *a*-axes. In (d) and (e) circles indicate orientations of *a*-axes, and thick great circles indicate prism planes with the highest Schmid factor, thick arrows indicate reorientation path for only basal slip; thin arrows indicate reorientation path for only prism slip. Contours for initial preferred orientation—3, 4 and 5%/1% area (a) Initial *c*-axis preferred orientation, great circles show orientations of prism planes (b) *c*-axis orientation (cross) for a single crystal after deformation primarily by rhomb slip. (c) *c*-axis orientation (cross) for a single crystal after deformation primarily by kinking. Note how the *c*-axis orientation of the crystal is closer to the shortening direction than for rhomb slip. (d) *c*-axis reorientation trajectories for a grain initially deformed by rhomb slip Prism slip (on plane with highest Schmid factor) causes the *c*-axis to move back towards approximately its original position. Basal slip causes the *c*-axis to move towards the shortening direction. (e) *c*-axes reorientation trajectories for a grain initially deformed primarily by kinking. In this new orientation the prism plane with the highest Schmid factor is changed. Prism slip causes the *c*-axis to move towards the centre of the stereonet, while basal slip causes the *c*-axis to move towards the shortening direction. The final *c*-axes location relative to the shortening direction is dependent on the combined basal/prism/rhomb slip activity

on this prism plane causes the *c*-axes to rotate towards the centre of the stereonet (i.e. towards the normal to the initial orientation of the lineation in the plane of the foliation; Fig. 15e). The final *c*-axis location then depends on the combined effect of basal and prism (with minor rhomb) slip, but will be located in the plane of the initial mylonitic foliation. This leads to an *a*-axis maximum normal to the initial lineation in the plane of the foliation, resulting in the greater extension observed in this direction in the specimen as a whole.

Specimens deformed 45SL

Specimens deformed 45SL show more complex reorientations. The superposition of deformation and specimen symmetries results in triclinic symmetry; this lower symmetry is observed in the resultant fabrics. Grains in maximum A on the side furthest from the shortening direction (position 3 in Table 2) have a higher Schmid factor on the prism plane than those grains closer to the shortening direction (position 1 in Table 2), but both have a uniformly high Schmid factor for rhomb slip. This change in the Schmid factor on basal and prism planes, and the high Schmid factor for rhomb slip, prevents the maxima from rotating as essentially distinct entities (as observed in the other orientations, particularly PSL); rather, individual grains may rotate in different directions. This results in the more complex fabrics observed.

There is some movement of grains from all maxima towards the shortening direction, predominantly by basal slip (e.g. G0193, Fig. 12). The final orientation will be dependent on the interaction of the three operating slip systems. As most grains have a high Schmid factor on the prism plane, *c*-axis maxima will generally develop at high angles to the shortening direction.

Specimen strength

The specimens deformed NSL and PSNL are appreciably stronger than those deformed PSL and 45SL. These stronger orientations also show minimal fabric changes. Slip systems in the stronger specimens are symmetrically disposed, as well as in comparatively stable orientations, with respect to the shortening direction; this prevents the slip systems from operating, leading to an increased strength. Strain is eventually accommodated by the formation of deformation and kink bands, with subsequent recrystallization. Deformation of recrystallized material produces fabrics resembling those of the starting material (in effect a stable end *c*-axis orientation).

Specimens deformed PSL and 45SL deform readily by the formation of kink bands and dislocation slip, leading to weaker specimens. Although slip planes are symmetrically oriented about the shortening direction for specimens deformed PSL, they are unstable with respect to the shortening direction, and deform readily. Kinking of grains in maximum A (Fig. 14) rapidly rotates basal planes from unfavourable orientations for basal slip into more favourable orientations for slip, resulting in weaker specimens.

CONCLUSIONS

Microstructures which develop during deformation of an anisotropic material (quartz mylonite) are broadly similar to those observed in deforming isotropic material (quartzite), namely strongly flattened grains with recrystallization becoming more important as temperature is increased and/or strain rate is decreased. The strength of the specimens decreases with increasing temperature and/or decreasing strain rate, although strength is also a function of specimen orientation with respect to the initial fabric of the mylonite. Specimens deformed PSL and 45SL are significantly weaker than those deformed NSL and PSNL. At 900°C and a strain rate of 10^{-6} s^{-1} strengths are similar for all orientations.

The strong orientations (NSL and PSNL) show minimal changes in fabric with deformation, while the weaker orientations (PSL and 45SL) show large fabric changes. The fabrics which develop depend on the relative contributions of the operative slip systems, which in turn depend on the initial specimen orientation. Deformation is accommodated by both the formation of kink bands within grains and dislocation slip. The fabrics are consistent with slip occurring only in the $\langle a \rangle$ direction, primarily on the basal and prism planes. Rhomb slip may occur if deformation cannot be fully accommodated by the previous mechanisms.

Contrary to previous geological studies (Kern 1977, 1979, Rutter & Rusbridge 1977) these experiments show that evidence for a previous deformation can be preserved to large strains. The reason for this difference is at present unknown. The operating deformation mechanisms in calcite (studied by Rutter & Rusbridge 1977) may be more efficient at erasing evidence for early strain than in quartz, whereas the fine grainsize of agate used in the studies by Kern (1977, 1979) may result in different deformation mechanisms to those used in the comparatively coarse-grained quartzite used in this study. Evidence for an earlier deformation is particularly well observed in specimens deformed PSL, which generally show asymmetric fabrics. Here the asymmetric maximum develops in the same quadrant as the asymmetric maximum in the initial fabric. The asymmetry can also be detected in specimens deformed NSL. This shows that after mylonites have been coaxially deformed, even to high strains, the sense of shear of the earlier deformation can still be determined if the deformation axes are symmetrically imposed on the specimen's axes of asymmetry. If the deformation axes are inclined to the specimen's axes, no definite fabric develops, and as such it may not always be possible to determine the initial sense of shear. The complex fabric pattern indicates a complex deformation history.

Acknowledgements—This work is a portion of a Ph.D. study undertaken by S. Ralser, with support provided by a Monash Graduate Scholarship. Laurel Goodwin and Joe White are thanked for critically reading the manuscript. Stefan Schmid and an anonymous referee are thanked for helpful reviews. Sample assemblies were skilfully produced by the mechanical workshop staff of Department of Earth Sciences, Monash University, under the direction of Les Jones. The Griggs rigs were maintained by the mechanical workshop staff at

Monash University, and by Alan White at CSIRO, Division of Geomechanics Robert Douglas made all the thin sections, often from very difficult specimens Graham Price is thanked for allowing use of the photometer, and helpful discussion Bob McCulloch is thanked for photographic work

REFERENCES

Avery, D H , Hosford, W F Jr & Backofen, W A. 1965 Plastic anisotropy in magnesium alloy sheets *Trans. metall. Soc* **233**, 71–78

Backofen, W. A 1972. *Deformation Processing*. Addison-Wesley, Reading, Massachusetts

Blacic, J D 1975 Plastic deformation mechanisms in quartz The effect of water *Tectonophysics* **27**, 271–294

Carreras, J., Estrada, A & White, S 1977. The effects of folding on the *c*-axis fabrics of a quartz mylonite. *Tectonophysics* **39**, 3–24

Evans, D J. & White, S. H 1984. Microstructural and fabric studies from rocks of the Moine Nappe Eriboll, NW Scotland *J Struct Geol.* **6**, 369–389

Green, H W , Griggs, D. T & Christie, J. M 1970. Syntectonic and annealing recrystallization of fine grained quartz aggregates In: *Experimental and Natural Rock Deformation* (edited by Paulitsch, P). Springer, New York, 272–335.

Hobbs, B E 1985. The geological significance of microfabric analysis. In: *Preferred Orientation in Deformed Metals and Rocks: An Introduction to Modern Texture Analysis* (edited by Wenk, H.-R) Academic Press, New York, 463–484.

Hosford, W. J Jr & Backofen, W. A 1964 Strength and plasticity of textured metals. In: *Fundamentals of Deformation Processing* (edited by Backofen, W A , Burks, J. J., Coffin, L. F Jr, Reed, N L. & Weiss, V.). Syracuse University Press, 259–298

Kern, H 1977. Preferred orientation of experimentally deformed limestone marble, quartzites and rock salt at different temperatures and states of stress *Tectonophysics* **39**, 103–120

Kern, H. 1979. Texture development in calcite and quartz rocks deformed at uniaxial and real triaxial states of strain. *Bull. Minéral* **102**, 290–300

Kocks, U. F. & Canova, G R. 1981. How many slip systems, and which? In. *Deformation of Polycrystals and Microstructures* (edited by Hansen, N., Horsewell, A , Leffers, T. & Lilholt, H.) Second Riso Int Symp. on Metallurgy and Materials Science, 35–44

Kocks, U F. & Chandra, H. 1982. Slip geometry in partially constrained deformation *Acta metall.* **30**, 695–709

Kronenburg, A. K & Tullis, J. A. 1984. Flow strengths of quartz aggregates: grain size and pressure effects due to hydrolytic weakening. *J geophys. Res.* **89**, 4281–4297.

Linker, M F., Kirby, S. H , Ord, A & Christie, J M 1984 Effects of compression direction on the plasticity and rheology of hydrolytically weakened synthetic quartz crystals at atmospheric pressure *J geophys Res* **89**, 4241–4255

Lister, G. S & Hobbs, B E 1980 The simulation of fabric development during plastic deformation and its application to quartzite the influence of deformation history *J Struct Geol* **2**, 355–370

Lister, G S & Williams, P F 1979 Fabric development in shear zones. theoretical controls and observed phenomena *J Struct Geol* **1**, 283–297

Lister, G S., Paterson, M. S & Hobbs, B E. 1978 The simulation of fabric development in plastic deformation and its application to quartzite: The model *Tectonophysics* **45**, 107–158

Mecking, H 1985 Textures of metals. In: *Preferred Orientation in Deformed Metals and Rocks: An Introduction to Modern Texture Analysis* (edited by Wenk, H -R) Academic Press, New York, 267–306

Ord, A. & Hobbs, B E. 1986 Experimental control of the water-weakening effect in quartz In *Mineral and Rock Deformation Laboratory Studies—The Paterson Volume* (edited by Hobbs, B. E. & Heard, H. C.) *Am Geophys. Un. Geophys. Monogr.* **36**, 51–72

Phillips, F C 1945 The microfabrics of the Moine Schists *Geol Mag* **82**, 205–240

Price, G P. 1979 The analysis of quartz *c*-axis fabrics by the photometric method. *J. Geol.* **88**, 181–195.

Ralser, S. 1990. Shear zones developed in an experimentally deformed quartz mylonite. *J. Struct. Geol.* **12**, 1033–1045

Rutter, E. H. & Rusbridge, M. 1977. The effects of non-coaxial strain paths on crystallographic preferred orientation development in the experimental deformation of a marble *Tectonophysics* **39**, 73–86

Schmid, S M. & Casey, M. 1986. Complete texture analysis of commonly observed quartz *c*-axis patterns. In: *Mineral and Rock Deformation: Laboratory Studies—The Paterson Volume* (edited by Hobbs, B E. & Heard, H C). *Am. Geophys Un. Geophys. Monogr.* **36**, 263–286

Simpson, C 1980. Oblique girdle orientation patterns of quartz *c*-axis from a shear zone in the basement core of the Maggia Nappe, Ticino, Switzerland. *J. Struct Geol.* **2**, 243–247

Sowerby, R. & Johnson, W. 1975. A review of texture and anisotropy in relation to metal forming. *Mater. Sci Engng* **20**, 101–111.

Tullis, J , Christie, J. M & Griggs, D. T. 1973. Microstructures and preferred orientations of experimentally deformed quartzites. *Bull geol Soc Am* **84**, 297–314.

Turner, F J & Weiss, L. E 1963. *Structural Analysis of Metamorphic Tectonites* McGraw-Hill, New York

Van Houtte, P. & Wagner, F. 1985. Development of textures by slip and twinning. In: *Preferred Orientation in Deformed Metals and Rocks An Introduction to Modern Texture Analysis* (edited by Wenk, H -R.). Academic Press, New York, 233–258.

Van Roermund, H., Lister, G S & Williams, P. F 1979 Progressive development of quartz fabrics in a shear zone from Monte Mucrone, Sesia-Lanzo Zone, Italian Alps. *J Struct Geol* **1**, 43–52.